Radioactive Nanomaterials for Multimodality Imaging

Daiqin Chen[1,2], Casey A. Dougherty[1,2], Dongzhi Yang[1,2], Hongwei Wu[1,2], and Hao Hong[1,2,3]

[1]Department of Radiology, University of Michigan, Ann Arbor, Michigan; [2]Center for Molecular Imaging, University of Michigan, Ann Arbor, Michigan; and [3]Comprehensive Cancer Center, University of Michigan, Ann Arbor, Michigan

Corresponding Author:
Hao Hong
Department of Radiology, University of Michigan,
109 Zina Pitcher Place, A520 BSRB, Ann Arbor, MI 48109-2200;
E-mail: hahong@med.umich.edu

Key Words: radioactive nanomaterials, multimodality imaging, PET, SPECT, MRI, optical imaging, fluorescence, photoacoustic imaging, Raman imaging, review

Abbreviations: Iron oxide nanoparticles (IONPs), desferrioxamine (DFO), upconversion luminescence (UCL), multi-walled carbon nanotubes (MWCNTs), photoacoustic imaging (PAI), Cerenkov luminescence imaging (CLI), quantum dots (QD), fluorescence-mediated tomography (FMT), mesoporous silica nanoparticles (MSNs), Cerenkov resonance energy transfer (CRET), melanin nanoparticles (MNPs), upconversion nanoparticles (UCNPs), lymph node (LN), upconversion nanoparticle (UCNP), positron emission tomography (PET), U.S. Food and Drug Administration (FDA)

ABSTRACT

Nuclear imaging techniques, primarily including positron emission tomography and single-photon emission computed tomography, can provide quantitative information for a biological event in vivo with ultrahigh sensitivity; however, the comparatively low spatial resolution is their major limitation in clinical application. With the convergence of nuclear imaging with other imaging modalities like computed tomography, magnetic resonance imaging, and optical imaging, the hybrid imaging platforms can overcome the limitations of each individual imaging technique. Possessing versatile chemical linking ability and good cargo-loading capacity, radioactive nanomaterials can serve as ideal imaging contrast agents. Here, we provide a brief overview about the current state-of-the-art applications of radioactive nanomaterials in multimodality imaging. We present strategies for incorporation of radioisotope(s) into nanomaterials with the applications of radioactive nanomaterials in multimodal imaging. Advantages and limitations of radioactive nanomaterials for multimodal imaging applications are discussed. Finally, a future perspective of possible radioactive nanomaterial utilization is presented for improving diagnosis and patient management in a variety of diseases.

INTRODUCTION

Molecular imaging has become a powerful tool for diagnosis and staging of multiple diseases and longitudinal treatment response monitoring (1-3). Imaging techniques such as magnetic resonance imaging (MRI), computed tomography (CT), ultrasonography, optical imaging, and nuclear imaging are widely used in different clinical scenarios (4). However, each individual imaging modality has inherent drawbacks (5, 6); thus, obtaining precise diagnostic information could be hampered by the use of a single imaging modality (7). Combining the merits of multiple imaging methods can provide for improved functional/anatomical information to be obtained; thus, researchers are more often using multimodality imaging platforms for their synergistic readouts (8, 9).

Integration of nuclear imaging approaches with other imaging modalities (10, 11) is rapidly advancing, as nuclear imaging (eg, positron emission tomography [PET] and single-photon emission computed tomography [SPECT]) provides whole-body detection with unparalleled sensitivity, good tissue penetration, and quantitative capacity (12, 13), with extremely high clinical value (13, 14). However, PET and SPECT imaging suffer from poorer spatial resolution; thus, the integration of PET or SPECT with other imaging methods with high spatial resolution, such as CT (15-18), and more recently MRI (19), provides synergistic opportunities for improved clinical diagnosis and overall patient care (11, 20). An interesting fact is that not many standalone PET scanners have been sold in the marketplace since the introduction of PET/CT in 2001 (8); therefore, the combination of PET and CT has become the "gold standard" for oncological imaging. With better soft tissue contrast and lower radiation dose than CT, MRI becomes a new attractive choice to integrate with PET (21), and this integration can help to compensate for the low molecular sensitivity/specificity of MRI (22, 23). Optical imaging (eg, fluorescence), on the other hand, is less costly and provides real-time intraoperative guidance after the disease location is pinpointed by PET (or SPECT) (24).

Contrast agents, which can enhance image conspicuity for lesion detection, are desirable for improving molecular imaging sensitivity and specificity. For example, gadolinium (Gd) compounds (typically T1-weighted) and iron oxide materials (typically T2-weighted) are commonly used MRI contrast agents (25, 26). Because PET and SPECT imaging rely on the detection of

ISSN 2379-1381 http://dx.doi.org/10.18383/j.tom.2016.00121

Table 1. Representative Radioactive Nanomaterials for Multimodality Imaging

Core Nanomaterials	Physical Properties	Radiolabel Incorporation Method	Intrinsic Imaging Capacity	Utilization	Synthesis Cost	Representative References
Inorganic nanomaterials						
IONPs	Paramagnetic (T2 contrast, T1 contrast when size is small)	External chelator, isotope absorption, covalent linkage (^{18}F)	MRI	LN mapping, tumor detection	$	(53, 58-60)
Gold	Fluorescence, photoacoustic signal, SERS	External chelator, radioactive precursor	Fluorescence, PAI, CRET	Tumor targeting, image-guided surgery	$$	(44, 93, 95, 99)
QD	fluorescence	External chelator	Fluorescence, CRET	LN mapping, tumor detection/surgery	$	(79, 80, 89, 90)
Silica	Biocompatibility, ultrahigh cargo-loading capacity, biodegradability	External chelator, Isotope absorption	N/A	LN mapping, tumor detection/surgery (for C-dots), image-guided drug delivery	$	(86, 88)
Carbon nanomaterials	Photothermal, fluorescence, photoacoustic signal, Raman signal	External chelator,	Fluorescence	Tumor detection	$$ (fullerene can be $$$)	(25, 112)
UCNPs	luminescent	External chelator, radioactive precursor (doping)	UCL	LN mapping, tumor detection	$$$	(83, 103)
Mn-/Gd-containing nanomaterials	Paramagnetic (T1 contrast)	External chelator, radioactive precursor	MRI	Tumor targeting,	$$	(72, 113)
Organic nanomaterials						
Liposome	Biocompatibility, optimal pharmacokinetics	External chelator, isotope absorption	Fluorescence, MRI (intrinsic label)	Tumor targeting	$	(68, 115)
Polymers	Biocompatibility, versatile chemistry	External chelator, isotope absorption	Fluorescence, PET (intrinsic label)	Tumor targeting, image-guided drug delivery	$	(69, 114, 116)

Abbreviations: IONPs – iron oxide nanoparticles; MRI – magnetic resonance imaging; PAI – photoacoustic imaging; CRET – Cerenkov resonance energy transfer; LN – lymph node; UCNPs – upconversion nanoparticles; UCL – upconversion luminescence; PET – positron emission tomography; SERS – surface-enhanced Raman scattering; QD - quantum dots.

γ-photons (511 keV pair or spontaneous) emitted from radioactive isotopes (eg, ^{18}F [$t_{1/2}$ = 110 minutes], ^{64}Cu [$t_{1/2}$ = 12.7 hours], ^{89}Zr [$t_{1/2}$ = 78.4 hours], and ^{99m}Tc [$t_{1/2}$ = 6 hours]) (12-14), the administration of contrast agents is indispensable. For successful multimodal imaging, a contrast agent with reliable performance and detectability by each imaging modality will be preferred. To achieve this goal, nanomaterials are very promising contrast agent candidates (27-29). The main advantages of the nanomaterials include the following facts:

(1) Some nanomaterials are inherent contrast agents, for example, iron oxide nanoparticles (IONPs), which have received approval by the U.S. Food and Drug Administration (FDA) as MRI contrast agents (30, 31).
(2) Most nanomaterials possess large surface areas, so they can accommodate numerous contrast agent molecules, thereby increasing local concentration and detection sensitivity (32).
(3) Different functional groups or active sites on nanomaterials enable them to be chemically linked to contrast agents or disease-targeting ligands (33).
(4) Some nanomaterials can respond to specific stimuli (eg, heat, light, or pH fluctuation) for on-demand release of payloads, which may improve the contrast in a given region of interest where the stimuli exist (34).
(5) Nanomaterials can show selective accumulation in some disease sites. The well-known example is that nanomaterials with suitable size and morphology can distribute preferably at the tumor site through an enhanced permeation and retention effect (27).

Hence, multimodality imaging agents based on nanomaterials have undergone continuous improvements by research investigators (29).

An overview of the current state-of-the-art applications for radioactive nanomaterials as multimodality imaging contrast agents is provided in Table 1. With the extensive availability of PET scanners in clinics and the higher sensitivity of PET than of SPECT, we will focus more on the radioactive nanomaterials applicable for PET-multimodality imaging while also providing a brief summary on nanomaterials useful for SPECT. With the rapid development of each imaging technique and nanotechnology, we foresee that radioactive nanomaterials will eventually be adopted as irreplaceable clinical tools in the near future.

RADIOACTIVE NANOMATERIAL PRODUCTION

According to the chemical compositions, nanomaterials are classified into organic and inorganic nanomaterials. Common examples of organic nanomaterials include liposomes and polymers and dendrimers (35), and chemical compositions from

inorganic nanoparticle families include silica-, iron oxide-, gold-, and carbon-based nanomaterials (30, 36-38). Nanomaterials from both categories are useful tools for PET- or SPECT-fused multimodal imaging. To produce radioactive nanomaterials for imaging applications, the following 4 approaches have been undertaken to incorporate radioisotopes:

(1) An exogenous coordination compound (named a "chelator") is added to the nanomaterial for binding radioactive metal ions (39).
(2) Proton or neutron beams are used to bombard the given atoms inside the nanomaterials to create postsynthesis radiolabels (40).
(3) Radioactive precursors (or preradiolabeled building blocks) are used to form radioactive nanomaterials (41, 42).
(4) Isotope absorption or exchange is used for postsynthesis radiolabeling (43, 44).

Each isotope incorporation approach has its own advantages and limitations. The attachment of the radioactive metal ions via exogenous chelators is simple and efficient, and it can be achieved at a relatively low cost. However, the stability of the resulting radiolabels has been a significant concern for this method, as radiometals can potentially be released from the chelator by isotope transchelation, and chelators themselves can be dissociated from the nanomaterial via enzymatic interactions in vivo. Chemical instability can compromise accurate evaluation of the pharmacokinetic behavior of radioactive nanomaterials in vivo. Direct radiolabeling methods by proton/neutron bombardment can largely avoid the above concerns, but the high cost and complicated instrumentation hinders practical use (40). Although the radioactive precursor method can form highly stable radioactive nanomaterials for imaging applications, unfortunately, the high radiation exposure during the production procedures is a significant working hazard (45). The chelator-free postsynthetic radiolabeling approach is a recently emerging method with low production cost and simplicity, although the stability and production yield of the resulting radioactive nanomaterials requires further improvement, and its application is currently limited to only a few nanomaterials. For future development, an optimal production method for radioactive nanomaterials should have high yields, stable products, short reaction times, low radiation exposure, and be easily adaptable to most nanomaterials (45). Development of new production methods and improvements of current strategies will promote new applications of radioactive nanomaterials. The current review presents an overview of the nanomaterials used in the context of their applicable imaging modality, as shown in Scheme 1.

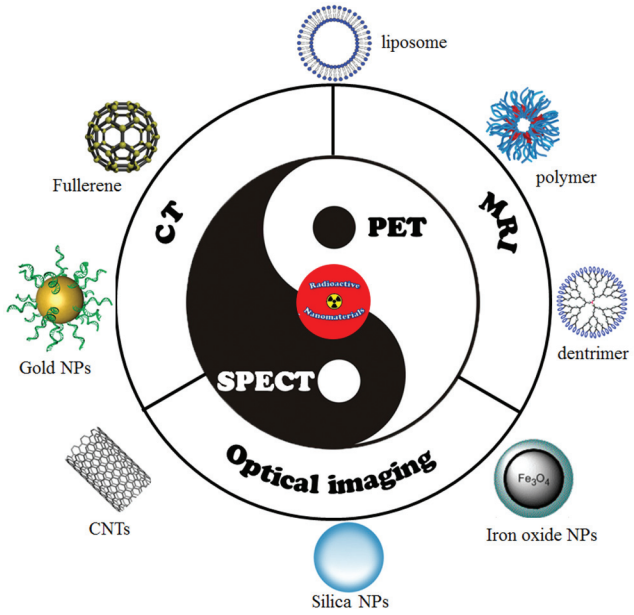

Scheme 1. Schematic illustration of radioactive nanomaterials for multimodality imaging.

MULTIMODALITY IMAGING WITH RADIOACTIVE NANOMATERIALS

PET/MRI

The first instrument to combine PET and MRI was developed in 2008 (19). Currently, both functional and anatomical data can be simultaneously collected by a modern PET/MRI scanner (46). Integration of PET and MRI endows the system with both high resolution and high sensitivity; thus, precise localization of the radioactive signals can be visualized within the context of anatomical features. Although a significant technical challenge, MRI can now provide attenuation correction for PET with clinically acceptable accuracy compared with CT-based attenuation correction (47-49). Because of the sensitivity differences between the 2 imaging modalities, dual-modality contrast agents must consider the need to maintain a relatively low concentration of PET contrast (usually within the nanomolar range) along with a relatively high concentration of MRI contrast agent needed for sufficient MRI detection. Therefore, radioactive nanomaterials used in PET/MRI applications should ideally contain a sufficiently high MRI contrast ability along with a sufficient dose of radioactivity for PET detection. As a standout example, IONPs coupled with different isotopes served as the core of many PET/MRI imaging nanoplatforms (30).

IONPs. Since IONPs have been approved by the FDA as clinically usable contrast agents for MRI (commercial name ferumoxytol), radioactive IONPs serve as the most popular PET/MRI agents (50). Given the fact that benefits and limitations of radiolabeled IONPs as dual-modality SPECT/MRI and PET/MRI imaging probes have already been summarized elsewhere (51), here we will briefly provide recent examples of IONP applications. ^{89}Zr (zirconium-89), a PET isotope with a decay half-life (78.4 hours), is well matched to the circulation half-lives of antibodies or nanomaterials; as such, it is considered clinically relevant and has been reported in significant research activities over the last decade (52). ^{89}Zr-labeled ferumoxytol was recently used for PET/MRI mapping of tumor-drained lymph nodes (LNs) in mice, as LN invasion is both critical for cancer staging and important for treatment planning (53). ^{89}Zr was attached to ferumoxytol via ultrastable coordination with desferrioxamine (DFO) (Figure 1A), and the modification of ferumoxytol core with ^{89}Zr–DFO did not alter its physicochemical properties such as size, charge, and magnetic properties. ^{89}Zr–DFO–ferumoxytol provided sensitive tomographic detection of the tumor-drained

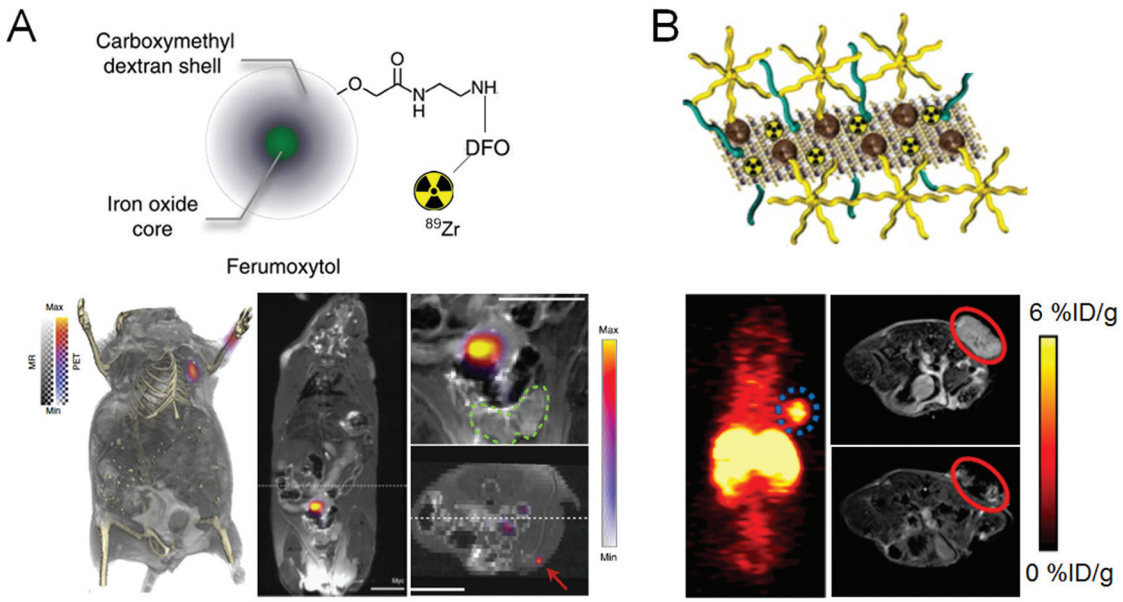

Figure 1. The application of ^{89}Zr-ferumoxytol for normal lymph nodes (LNs) and tumor-drained LNs (A). Top panel: the structure of ^{89}Zr-ferumoxytol. Lower left panel: detection of normal axillary LNs by ^{89}Zr-ferumoxytol in positron emission tomography (PET)/magnetic resonance imaging (MRI). Lower middle panel: detection of the tumor-drained LN in Hi-Myc mouse by ^{89}Zr-ferumoxytol in PET/MRI. Down right upper panel: PET/MRI of prostate region showing that the drained LN is outside of the prostate organ (green circle). Down right lower panel: distant drained inguinal node is identified by ^{89}Zr-ferumoxytol (red arrow). Reproduced with permission from Thorek et al (53). The application of ^{64}Cu-labeled, MoS_2/IONP hybrid nanomaterial for PET- and MRI-based tumor detection (B). The structure of ^{64}Cu-labeled MoS_2/IONP is shown along with PET and MRI results at 24-hour after injection. Significant tumor uptake was confirmed in PET (circle indicates the tumor location) with a "darkened" tumor area in the MRI. Reproduced with permission from Liu et al (62).

axillary LNs in prostate tumor-bearing mice with high resolution (Figure 1A). Compared with the commonly used agent (^{99m}Tc-radiocolloid) for LN mapping, ^{89}Zr–DFO–ferumoxytol shortened the diagnosis time and decreased the radiation dose to the test subjects. The IONP-based platform has significant translational potential to improve preoperative planning for nodal resection and tumor staging. By coupling with different PET isotopes (eg, ^{64}Cu, ^{124}I, ^{72}As, and ^{69}Ge), successful LN mapping was also achieved with these radioactive IONPs (54-57).

Aside from LN mapping, radioactive IONPs can also be used for in vivo cancer targeting. For example, arginine–glycine–aspartic (RGD, a potent ligand for integrin $\alpha_v\beta_3$) peptide-conjugated ^{64}Cu-labeled IONPs could efficiently accumulate inside different types of tumors and give clear tumor delineation in both PET and MRI (58-60). More recently, hybrid nanostructures of IONPs [eg, with aluminum hydroxide (labeled with ^{18}F) (61) or MoS_2 nanosheets (labeled with ^{64}Cu; Figure 1B) (62)] were also prepared for cancer imaging and subsequent image-guided cancer therapies. IONPs-based PET/MRI agents still possess certain drawbacks. Because IONPs are mostly used as T2-weighted contrast agents (negative contrast), image interpretation can be relatively difficult. Another concern is the aggregation of IONPs in vivo, which can alter the local signal intensity from MRI. A recent study demonstrated that aggregated IONPs, instead of IONPs alone, could produce significant artifacts in magnetic resonance (MR)-derived attenuation correction maps from PET/MRI (63). To overcome these limitations, T1-weighted contrast agents, for example, Gd and manganese (Mn) complexes, may be more preferred.

Gadolinium-Containing Nanomaterials. Gd-containing nanomaterials are attractive MRI probes as long as proper functionalization has been conducted to maintain material integrity and prevent leakage of Gd ions. As an image contrast platform, the applicability of Gd oxide nanoparticles in PET/MRI and therapeutic delivery has been recently reviewed (64).

Fullerene is also a well-known delivery vector of Gd (38). A PET/MRI probe based on ^{124}I-labeled $Gd_3N@C_{80}$ fullerene derivative was developed, and potential cytotoxicity from Gd leakage was avoided by caging the Gd ions inside the fullerene structure (25). Not only can this biocompatible $Gd_3N@C_{80}$ be used as a T1-weighted MRI agent and PET probe, it can also serve as a "radical sponge" to ameliorate inflammatory responses. Hydroxyl and carboxylic groups on the surface of $Gd_3N@C_{80}$ are also useful, as they allow the capability of additional functionalization. Tumors inside the glioblastoma-bearing rats could be distinctly visualized by ^{124}I-labeled $Gd_3N@C_{80}$ from both PET and MRI. Rare-earth nanomaterials are another category of suitable nanoplatform for PET/MRI applications (65). Among them, Eu^{3+}-doped Gd vanadate ($GdVO_4$:Eu) nanosheets that have been synthesized by a solvothermal reaction in 1 study and further modified by 1,4,7,10-tetraazacyclododecane-1,4,7,10-tetraacetic acid (DOTA) for ^{64}Cu labeling and Asp-Gly-Glu-Ala (DGEA) peptide for integrin $\alpha_2\beta_1$ cellular targeting (66). Prominent accumulation of ^{64}Cu-DOTA-$GdVO_4$:Eu-DGEA in PC-3 tumors (integrin $\alpha_2\beta_1^+$) was confirmed by both PET and MRI (Figure 2A), and tumor uptake was primarily mediated by integrin $\alpha_2\beta_1$ targeting. In an interesting study, a ^{64}Cu-labeled hybrid nanomaterial based on gold, Gd, and IONP was

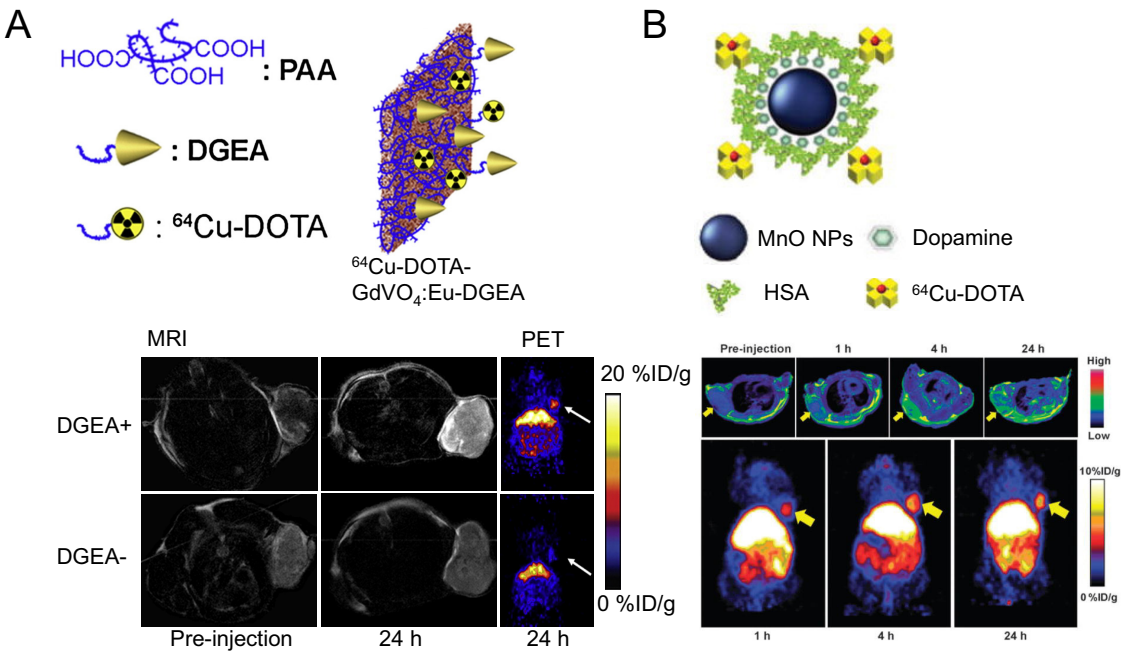

Figure 2. Application of ^{64}Cu-labeled $GdVO_4$: Eu nanosheets for targeted tumor imaging (A). The schematic structure of ^{64}Cu-DOTA-$GdVO_4$: Eu nanosheets is shown. PET and MRI images of PC-3 (EphB4$^+$) tumor-bearing mice at 24-hours after injection are shown for ^{64}Cu-DOTA-$GdVO_4$: Eu nanosheets with or without conjugation of the Asp-Gly-Glu-Ala (DGEA) peptide. Reproduced with permission from Hu et al (66). Application of ^{64}Cu-labeled MnO@HSA nanoparticles for MRI and PET imaging of tumors (B). Upper panel: magnetic resonance (MR) images on U87MG xenografts acquired at 0, 1, 4, and 24 hours after ^{64}Cu-labeled MnO@HSA injection. Lower panel: PET images taken at 1, 4, and 24 hours after ^{64}Cu-labeled MnO@HSA injection. Reproduced with permission from Huang et al (72).

used for dual T1- and T2-weighted MRI and PET to delineate tumors (67). The resultant hybrid heterotrimers showed high physiological stability and could induce simultaneous positive and negative contrast enhancements in MR images. PET imaging studies revealed that the hybrid heterostructures showed favorable tumor delineation in mice, consistent with the MRI findings.

There are rather limited reports available on Gd-containing organic nanomaterials as PET/MRI agents. One such example is Gd-containing liposome (68). In this study, Gd was introduced via diethylenetriaminepentaacetic acid coordination, and ^{89}Zr was incorporated by adsorption on lipid membranes. Octreotide, a peptide targeting human somatostatin receptor subtype 2 (SSTR2), was also linked to the liposome complex. Clearly, higher accumulation and retention in SSTR2$^+$ tumors (acquired from PET/MRI), when compared with SSTR2$^-$ tumors in the same animal, were strong evidence that these ^{89}Zr/Gd-containing liposomes showed excellent tumor-targeting ability in vivo. More recently, a glucose-based polymeric dextran nanomaterial (named "nanobeacon" by the authors) was also developed to retain ^{89}Zr and Gd in a chelator-free manner (69). These ^{89}Zr-nanobeacons could detect sentinel LNs and allow the surveillance of drug release from nanobeacons via MRI, as the MR signal from Gd could be quenched by the loaded drug on the nanobeacons.

Manganese-Containing Nanomaterials. The T1-shortening properties qualify manganese as an MRI contrast agent (70). However, its biological toxicity hampered the development of otherwise useful applications such as cancer imaging, cell tracking, and brain imaging (71). Unlike Gd, an effective chelating agent with satisfactory binding stability for manganese has unfortunately not yet been identified for in vivo applications. Manganese-containing nanomaterials with sufficient in vivo stability may grant new biomedical applications to manganese. Surprisingly, using manganese-containing nanomaterials for PET/MRI is a current underexplored niche in contrast agent imaging research.

To the best of our knowledge, only 1 existing report has used ^{64}Cu-labeled human serum albumin (HSA)-coated MnO nanoparticles for PET/MRI imaging of glioblastoma (72). The coating of HSA can increase the solubility of MnO nanoparticles and their longitudinal R_1 relaxivity. These ^{64}Cu-labeled MnO@HSA nanoparticles showed good physiological properties and stability along with superior T1 contrast. Tumor accumulation from ^{64}Cu-labeled MnO@HSA was confirmed by both PET and MRI (Figure 2B). There are numerous opportunities ahead for manganese-containing nanomaterials to be used in PET/MRI studies, as the production of ^{52}Mn ($t_{1/2}$ = 5.6 days) has been optimized for PET applications (73). For future development, radiolabeled, hollow MnO nanoparticles (with better water accessibility) and stimulus-responsive manganese-containing nanomaterials are anticipated to be useful for improving both contrast agent sensitivity and specificity for detection of specific stimuli (74).

PET/Optical

PET/Fluorescence (Luminescence). The combination of PET and fluorescence/luminescence provides opportunities for radioactive nanomaterials to be used for fluorescence-/lumines-

cence-guided surgery after initial detection of the disease site(s) via PET. There are 3 categories of radioactive nanomaterials that are useful for PET/fluorescence. In the first category, the nanomaterial has intrinsic fluorescence (eg, quantum dots [QD], gold nanomaterials and upconversion nanoparticles [UCNP]), which can be used for PET/fluorescence after direct radiolabeling. The second category involves nanomaterials labeled with both a radioisotope and a fluorophore. Sometimes, the loaded drugs (eg, doxorubicin) on the nanomaterial can also serve as a fluorophore for imaging purposes (75-77). A third category involves radioactive nanomaterials that can be detected by both PET and Cerenkov luminescence imaging (CLI) from the same radiolabel. CLI is an emerging optical imaging modality based on the detection of Cerenkov radiation induced by particles emitted by a radioisotope as they travel through biological samples with a velocity faster than the speed of light (78). The progress in these 3 categories will be the focus of this section.

Radiolabeled QDs are the most prevalent nanomaterials for PET/fluorescence. QDs with different radiolabels [eg, ^{64}Cu (79, 80) or ^{18}F (81)] have been used for PET/fluorescence imaging of tumor vasculature with consistent readouts from both PET and fluorescence imaging modalities. Rare-earth UCNP is another type of nanomaterial with unique intrinsic fluorescence. It can absorb low-energy photons and emit high-energy photons (upconversion luminescence [UCL]), resulting in a very optimal signal-to-background ratio for imaging (82). UCNPs are ideal building blocks for multimodal imaging probes. For example, ^{18}F-labeled, cyclodextrin-coated UCNPs were used for cell labeling and in vivo LN imaging via UCL/PET (83). The good biocompatibility from UCNPs encourages their use as multimodal imaging probes, although more reliable instrumentation will likely be needed for applications in UCL imaging. Other candidates such as red fluorescence-emitting zinc oxide nanoparticles (84) can also be useful for PET/fluorescence.

Postsynthesis incorporation of both fluorophore and radioisotopes is the most frequently adopted technique to produce PET/fluorescence-suited nanomaterials. For example, fluorescence-mediated tomography and PET were used to simultaneously measure protease activity, macrophage content, and integrin expression in the tumor by using a biocompatible IONP with ^{18}F and a near-infrared (NIR) fluorophore (NIRF) attachment (85). Good correlations were shown between fluorescence-mediated tomography and PET in probe concentration and spatial distribution of signals.

Silica-based nanomaterials are important for PET/fluorescence imaging, where ample attention has been devoted on mesoporous silica nanoparticles (MSNs) and ultrasmall silica-based Cornell dots (C-dots). MSNs conjugated with ^{64}Cu, 800CW (an NIRF dye), and a monoclonal antibody were adopted for PET/NIRF imaging of the tumor vasculature in 1 study (86). Good tumor-targeting efficacy and specificity in breast tumor-bearing mice were achieved for this ^{64}Cu-labeled MSN, validated by PET and fluorescence. C-dots are the first PET/fluorescence nanoprobes that entered the clinical stage testing. After conjugation with ^{124}I, an NIRF fluorophore (Cy5), and RGD peptide, C-dots were used as an integrin-targeting platform for imaging of melanoma metastasis with improved SLN (sentinel lymph node) localization and retention (Figure 3A), target-to-background ratios, and fast clearance from the site of injection and the body (87). The specificity of this C-dots platform, when compared with that of ^{18}F-FDG, for metastasis/inflammation discrimination, was also satisfactory in the setting of surgery and therapeutic intervention. Furthermore, these radiolabeled C-dots were also used in a first-in-human clinical trial for lesion detection, cancer staging, and treatment management of patients with metastatic melanoma (88). ^{124}I-RGD-C-dots(Cy5) showed superior in vivo stability, reproducible pharmacokinetic signatures (renal excretion), good tolerance in patients, and sensitive detection of small metastatic lesions (Figure 3A).

As stated previously, CLI enables the use of widespread luminescence rodent imaging equipment (eg, IVIS Spectrum) to visualize many commonly used medical isotopes (78), including clinical diagnostic (eg, PET) and therapeutic radionuclides. Compared with conventional optical imaging agents, CLI enables the use of approved radiotracers and does not require an external light excitation source, which would result in its rapid translation to clinical applications combining PET imaging and CLI-guided surgery with PET tracers. An emerging concept is to produce self-illuminating imaging agents (Cerenkov luminescence from isotopes served as the excitation source—named Cerenkov resonance energy transfer [CRET]) without autofluorescence background interference. Currently, only a few self-illuminating probes were developed, based mainly on QDs (89, 90), and $^{64}CuCl_2$ was used as a synthesis precursor. These ^{64}Cu-doped QDs showed excellent radiochemical stability and potent tumor uptake (Figure 3B), and these were successfully applied as efficient imaging agents for PET/self-illuminating luminescence in vivo. Radioactive gold nanocluster (^{64}Cu-doped AuNCs) was another strong competitor for CRET-based PET/NIRF imaging (44), in which AuNCs acted as the energy acceptor for NIR fluorescence. ^{64}Cu-doped AuNCs showed efficient CRET–NIR and PET signals, better passive targeting to tumors, and lower toxicity than QD conjugates. Although these studies were conducted in a preclinical setting (mostly mouse studies), the successful clinical translation of CLI-nanomaterials can be expected in the future, which will catapult radioactive nanomaterials toward increasingly versatile applications (91).

Other PET/Optical Imaging. Compared with fluorescence imaging, other optical imaging techniques, such as Raman imaging or photoacoustic imaging, can also provide opportunities for integration as hybrid imaging applications with PET. Since its discovery, Raman spectroscopy, based on the inelastic scattering of a photon, has proven to be a powerful analytical tool offering many advantages including excellent sensitivity to small structural and chemical changes, its ability to multiplex, and its resistance to both autofluorescence and photobleaching (92). Although both radiolabeled noble metal nanomaterials and carbon nanomaterials can be used for PET/Raman imaging, most of the time Raman imaging is only a safeguard to ensure that material distribution information collected from PET is accurate. For example, the organ distribution of ^{64}Cu-labeled gold nanoparticles was evaluated in mice by PET and validated by ex vivo Raman imaging via surface-enhanced Raman scattering (93). Raman imaging of excised tissues correlated well with distribution data from PET in this study (Figure 4A). The benefit of fusing Raman images onto PET images is that this combination can provide simultaneous surveillance of different materials/substances (with distinct Raman emissions) with excellent sensitivity (PET and Raman).

Photoacoustic imaging (PAI), based on the photoacoustic effect, is another attractive optical imaging technique with non-ionizing electromagnetic waves, good resolution and contrast, portable instrumentation, and the ability to partially quantify the signal. PAI has been applied to the imaging of cancer, neurological disorders, vasculature function, and gene expression, among others (94). An anisotropic branched gold nanoma-

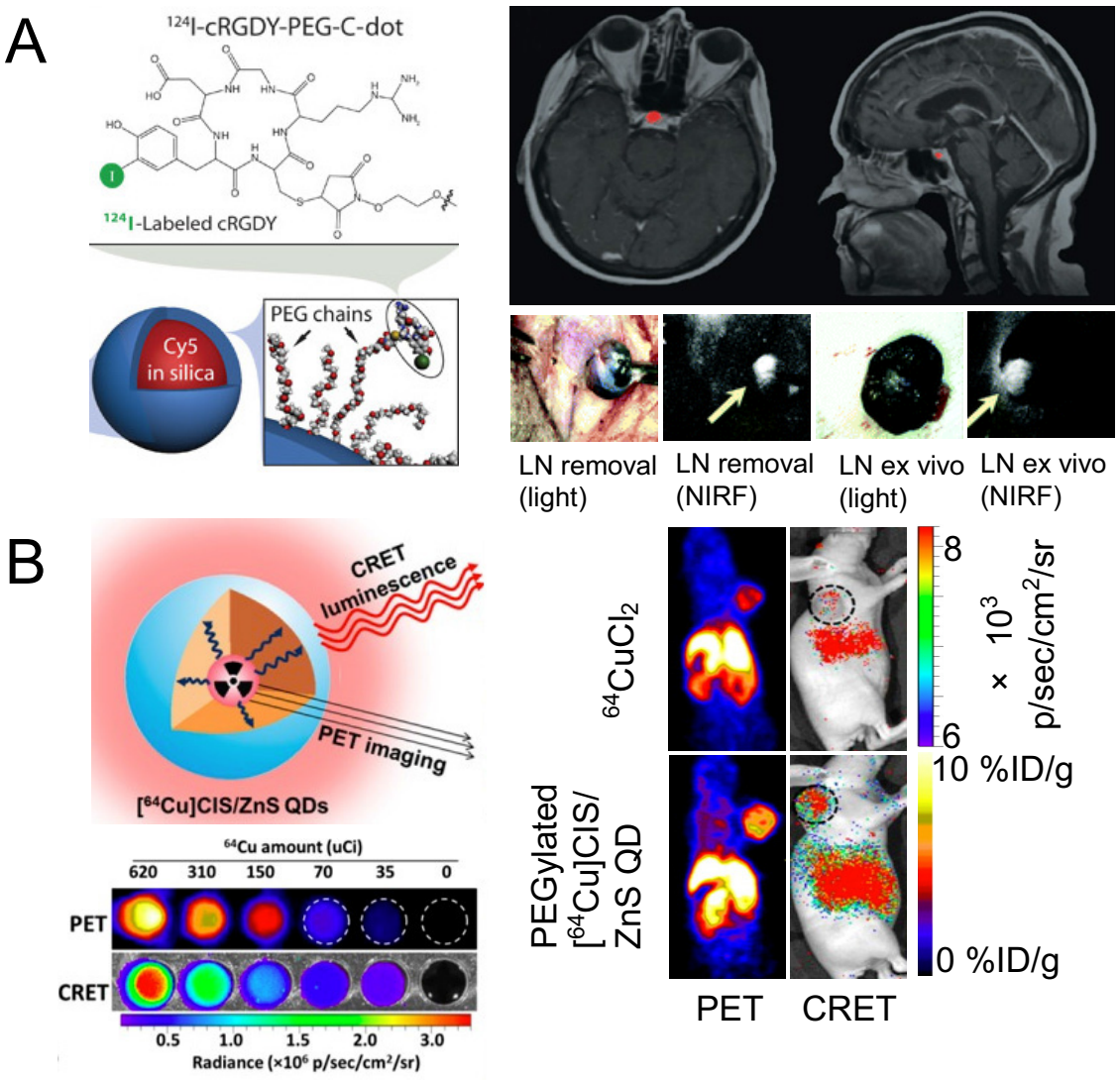

Figure 3. Application of ^{124}I-labeled, arginine–glycine–aspartic (RGD)-conjugated Cornell dots (C-dots) for clinical cancer detection and near-infrared fluorophore (NIRF)-guided surgery (A). Biocompatible C-dots could delineate a small pituitary lesion in a patient with metastasis patient in PET/MRI. The same-structured C-dots were successfully used for NIRF-guided tumor-drained LN removal. Reproduced with permission from Bradbury et al and Phillips et al (87, 88). Structure and application of intrinsically radioactive ^{64}Cu-QDs for PET and Cerenkov resonance energy transfer (CRET) imaging (B). CRET luminescence photon flux was in a linear correlation with incorporated radioactivity. Consistent tumor uptake in U87MG tumors was revealed by PET and CRET. Reproduced with permission from Guo et al (90).

terial (Au-tripods) with superior optical properties was developed for PET/PAI (95). A linear correlation between PAI signals and Au-tripods concentration was confirmed in vivo. Intravenous administration of ^{64}Cu-labeled, RGD peptide-conjugated Au-tripods (RGD–Au-tripods) to U87MG tumor-bearing mice showed PAI contrast in tumors almost 3-fold higher than for the blocking group, and PAI results correlated well with corresponding PET images. Au-tripods showed adequate selectivity and sensitivity for tumors in PET/PAI. In another study, the intrinsic PA signals and strong chelating properties (eg, for ^{64}Cu) of melanin nanoparticles (MNP) were exploited to construct a PET/MRI/PAI agent (96). With apoferritin conjugation for transferrin receptor 1 (TfR1) targeting, this MNP showed excellent stability and presented good tumor uptake and high tumor contrast in HT29 tumor (TfR1$^+$), with significantly lower accumulation in HepG2 (TfR1$^-$; Figure 4B).

Multimodality Imaging

Multimodality imaging platforms that combine more than 2 different imaging modalities have come into research focus (97, 98). To achieve this, nanomaterials used are usually in a hybrid structure or a core/shell architecture to embrace more contrast capacity from different components (99-101).

Cui et al proposed 2 core–shell nanomaterials for trimodal (MRI, PET/SPECT and optical) imaging based on the integration

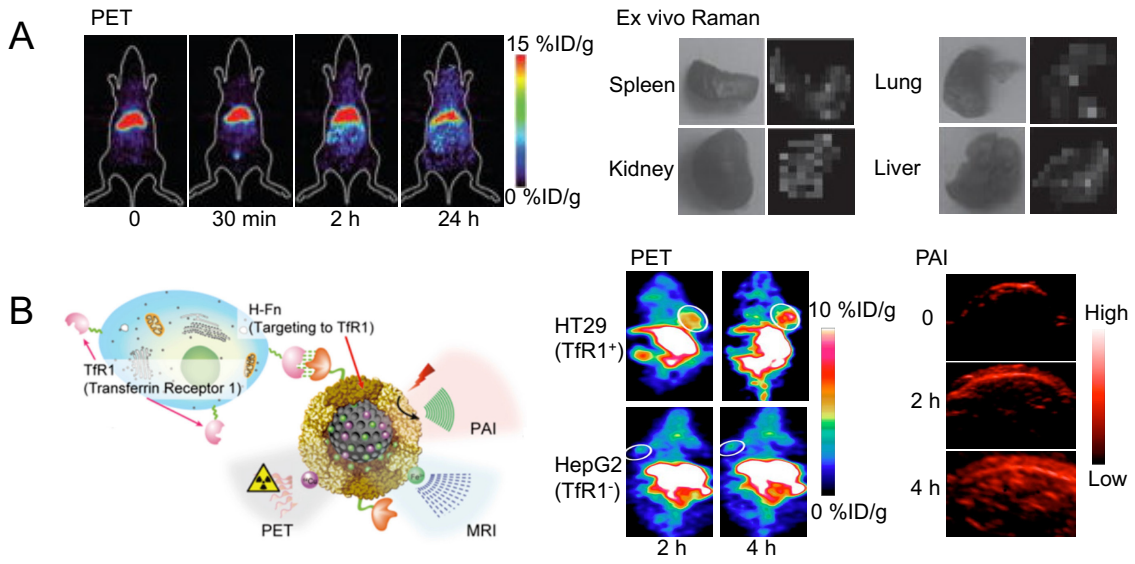

Figure 4. PET and ex vivo Raman imaging to evaluate the organ distribution of ^{64}Cu-labeled gold nanoparticles (A). Consistent organ uptake was obtained by PET and Raman signals. Reproduced with permission from Zavaleta et al (93). ^{64}Cu-labeled melanin nanoparticles were used for tumor detection via PET and photoacoustic imaging (PAI) (B). The schematic structure of melanin nanoparticles (MNPs) is provided along with examples of both PET and PAI images of tumor-bearing mice. Reproduced with permission from Yang et al (96).

of IONP and UCNP (102). The nanoparticles are composed of core–shell Fe_3O_4@$NaYF_4$ nanoparticles with different metal ions doped (Yb, Er, Tm, etc.). With the stabilization from polyethylene glycol, the obtained nanoparticles showed high transverse relaxivity (R_2) (326 $mM^{-1}s^{-1}$ at magnetic field of 3T), good radiolabel stability, and strong upconversion luminescence. LNs in live mice could be clearly visualized by using ^{18}F-labeled Fe_3O_4@$NaYF_4$ (Yb, Tm) nanoparticles in PET, MRI, and UCL. With a similar design, hybrid gold-IONP nanoparticles were made, in which IONPs worked as a T2 MRI contrast agent, and the gold component acted as a strong fluorescence emitter and functionalization site (modified with 1,4,7-triazacyclononane-1,4,7-trisacetic acid for ^{64}Cu labeling) (99). Anti-EGFR (EGFR stands for epidermal growth factor receptor) affibody was also included to provide tumor-targeting capabilities. As expected, the gold-IONP platform gave very sharp tumor contrast in PET, MRI, and fluorescence imaging. More recently, another more dramatic example is the hexamodal imaging by porphyrin–phospholipids-coated UCNP (PoP-UCNP) (103). To more fully utilize the imaging capacity of this nanomaterial, the authors characterized it both in vitro and in vivo for imaging via fluorescence, upconversion, PET, CT, CLI, and PAI (Figure 5).

SPECT-Related Multimodality Imaging

For the last few decades, SPECT is the leading nuclear imaging technique because of the extensive use of ^{99m}Tc ($t_{[1/2]}$ = 6 hours), which can be conveniently obtained from ^{99}Mo/^{99m}Tc generators (104). It is more established, less expensive, and more widely available than PET. One of the major advantages of SPECT imaging is that it can be used for simultaneous imaging of different radionuclides via the energy identification of the gamma photons emitted (105), thereby enabling simultaneous visualization of parallel biological events, although such strategy is not frequently adopted. From a material point of view, the key differences between a PET- and a SPECT-applicable nanomaterial are the specific radioisotopes used. Because PET possesses certain superiority (eg, higher detection sensitivity, better spatial resolution, and better quantitative capacity) and has become increasingly popular in both preclinical and clinical settings, SPECT-applicable nanomaterials will not be discussed in detail in this paper. Similar to PET isotope-included nanomaterials, radioactive nanomaterials can be used for SPECT/MRI and SPECT/optical, and additional combinations are possible (106-108).

SPECT/MRI can be extremely helpful in scrutinizing the in vivo kinetics of radioactive nanomaterials (20, 106, 109, 110). For example, in vivo metabolism of polyethylene glycol (PEG)-modified ultrasmall paramagnetic iron oxide nanoparticles (USPIO, 1 type of IONPs), after labeling by ^{99m}Tc, could be monitored by both SPECT and MRI (Figure 6A) (111). ^{99m}Tc-PEG-IONP possess a high R_1 relaxivity and a low R_2/R_1 to serve as an attractive T1-weighted MRI contrast agent. IONP-combined multiwalled carbon nanotubes (MWCNTs) were also used for SPECT/MRI after being further radiolabeled with ^{99m}Tc (112). Mouse imaging studies showed that the T2 contrast ability of superparamagnetic iron oxide nanoparticle (SPION)-MWCNTs was comparable with that of the clinically approved MRI contrast agent, Endorem. Organ distribution of SPION-MWCNTs acquired from SPECT, along with ex vivo transmission electronic microscopy and histological assessment, confirmed the integrity of SPION-MWCNTs in organs. Moreover, Gd-contain-

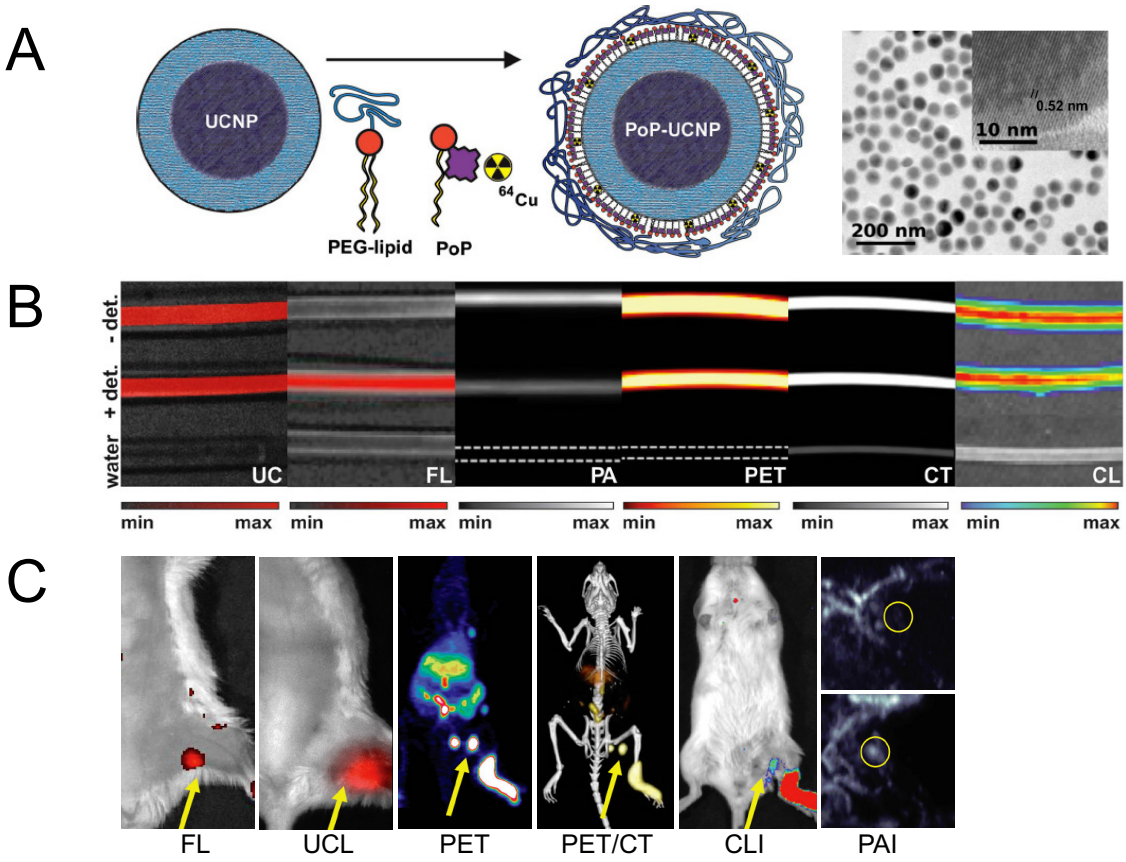

Figure 5. Hexamodal imaging with radioactive nanomaterials. Schematic structure and transmission electronic microscopy (TEM) images of this porphyrin-/lipid-wrapped upconversion nanoparticles (UCNPs) (A). Imaging studies with material-filling tubing by upconversion luminescence (UCL), fluorescence, PAI, PET, computed tomography (CT), and Cerenkov luminescence imaging (CLI) (B). Signal intensity–tissue depth relationship was also examined. (Note: +/− det means cover or remove turkey breast over the tubing). In vivo LN mapping by these 6 imaging modalities (C). Photoacoustic (PA) images before and after the material injection are shown. Reproduced with permission from Rieffel et al (103).

ing nanomaterials were also important participants in the SPECT/MRI studies. For example, hybrid Gd oxide nanoparticles (obtained by encapsulating Gd_2O_3 cores within a polysiloxane shell), which carried fluorophore Cy5 and (111) In, were used in SPECT, fluorescence, and MRI to evaluate their metabolism (eg, renal clearance) in rodents (113). A clear correlation was observed between modalities.

Many radioactive nanomaterials are useful for SPECT/fluorescence imaging or SPECT-involved multimodality imaging. Polymeric micelles conjugated with an EphB4 (a receptor tyrosine kinases overexpressed in many tumors)-binding peptide TNYL-RAW, an NIRF fluorophore Cy7, and ^{111}In was used for tumor imaging via SPECT and NIRF (114). PC-3M tumors (EphB4$^+$) could be clearly visualized by both SPECT and NIRF tomography after intravenous administration of ^{111}In-labeled TNYL-RAW-micelles (Figure 6B). EphB4 specificity was confirmed from tumor uptake in A549 tumors (EphB4$^-$) and blocking experiments. Fluorescence signal from the nanoparticles correlated with their radioactivity count and colocalized with the EphB4-expressing region from histology. Liposomes incorporated with fluorescence labels and Gd or ^{111}In were investigated in optical, MRI, and SPECT imaging for their cellular uptake and organ distribution (115). The ability to tune the imaging properties and distribution of these liposomes allows for the future development of a flexible trimodal imaging agent. Other more recent progress includes optically tunable nanomaterials featuring a unique design, where a single PEG polymer surrounds a fluorophore- and radiometal-bearing peptide (116). These nanomaterials could be applied for intraoperative angiography, measurements of capillary permeability, and tumor visualization by SPECT, for potential patient stratification.

SUMMARY AND FUTURE PERSPECTIVES

There are 2 critical composing elements for a radioactive nanomaterial, that is, the radioisotope and the nanomaterial. For ready availability of radioactive nanomaterials for multimodality imaging, suitable selection of both components should be synergistic. On the one hand, incorporation of radioisotope(s) bestows extra tracking/therapeutic ability to the nanomaterial, which cannot be acquired by loading of other cargos. On the

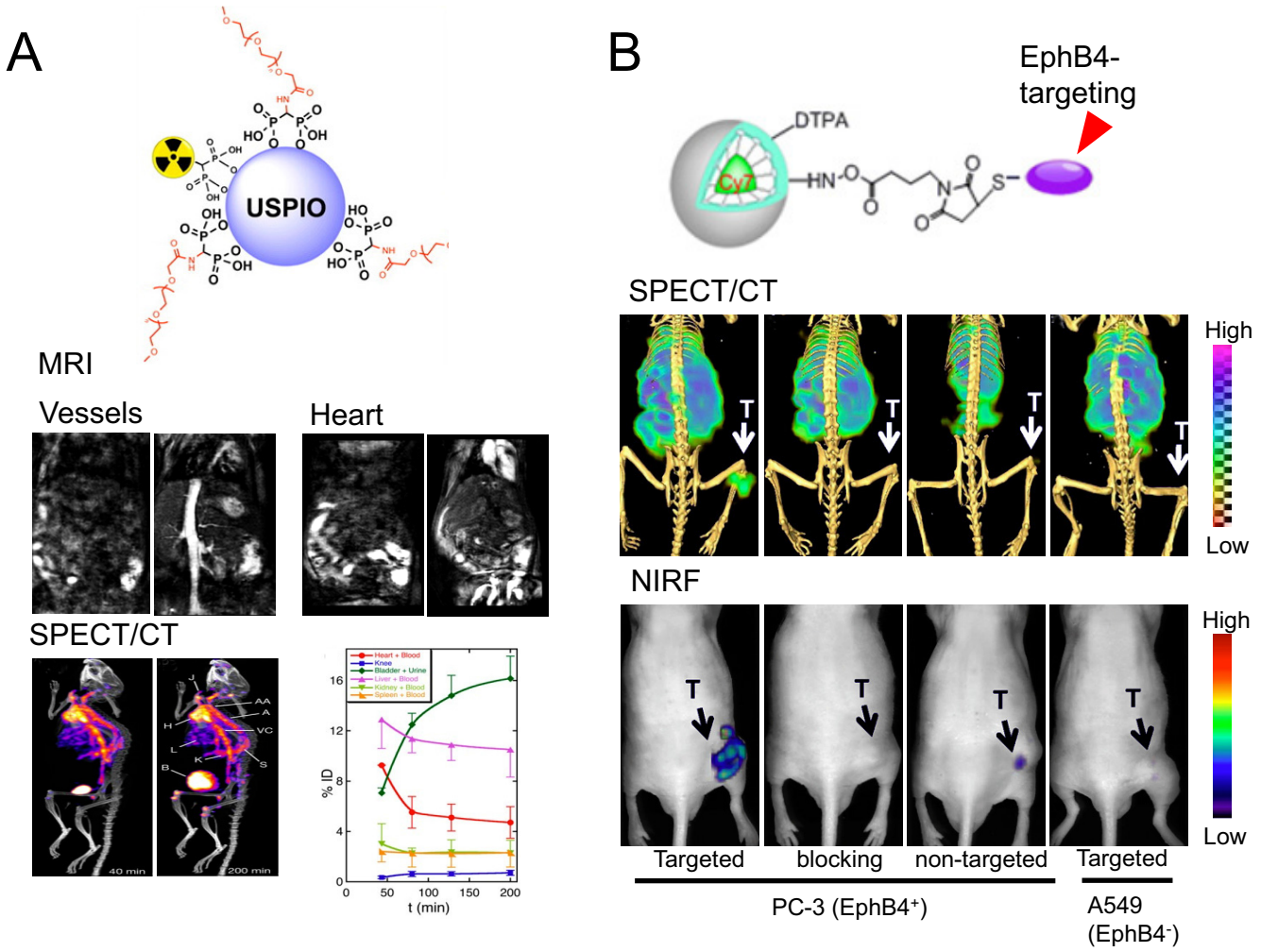

Figure 6. Schematic structure of ^{99m}Tc-labeled ultrasmall paramagnetic iron oxide nanoparticles (USPIOs) (an iron oxide nanoparticle [IONP]) and clarification of its organ distribution by SPECT and MRI. T1-weighted images showing the increase in signal from blood in the vessels and the heart. SPECT/CT demonstrated similar pharmacokinetic profile for the ^{99m}Tc-labeled USPIO. Reproduced with permission from Sandiford et al (111). Schematic structure of EphB4-targeting micelles and their applications in SPECT/NIRF imaging of EphB4$^+$ and EphB4$^-$ tumors (B). The EphB4 specificity of these micelles was validated by these two imaging modalities. Reproduced with permission from Zhang et al (114).

other hand, the utilization of suitable nanomaterials may serve as an isotope carrier and enable some unconventional isotopes to be used in specific biomedical applications, which may otherwise be very difficult to achieve, such as radioactive arsenic (eg, ^{72}As) (57, 117), gemanium-69 (^{69}Ge) (56), or sodium-22 (^{22}Na) (118). Different imaging "labels" can be integrated into a single nanoplatform for combining the strengths of different imaging modalities, which can synergistically improve the overall value of imaging in the context of either basic research or patient care. In addition, nanomaterials with appropriate functionalization can evade attack from the immune system and thus create prolonged imaging time (45). Moreover, because most nanomaterials have large surface areas, which result in superior cargo accommodating capacity, they can help to increase local imaging contrast in selected areas. In addition, loading of imaging labels (isotopes/fluorophores, etc.) in nanomaterials can cause alterations of the in vivo pharmacokinetics of the labels, which can be tunable for image optimization in most cases.

Each imaging modality has its own advantages and limits. For example, the high sensitivity and good quantitative capability provided by PET/SPECT accompanies their low spatial resolution (typical >1 mm). The inherent low sensitivity of MRI and penetration limitations from optical imaging calls for combining the strengths of different imaging modalities to synergistically improve the information content provided by imaging. When radioactive nanomaterials are used in multimodality imaging, their stability is one of the most crucial factors for detection reliability, accuracy, and safety. The concept of "stability" here has dual meanings—radiochemical stability and stability of the nanomaterial itself. To acquire reliable and comparable imaging results, all the cargo(s) (particularly the radio-

isotopes) should stay adequately stable within the nanomaterial structure during the in vivo application, as PET or SPECT identifies the location of radionuclides rather than nanomaterials. Alternate functionalization/engineering strategies can be applied to not only optimize the stability of radioactive nanomaterials but also to provide the possibility for conjugation of a diverse number of different biological and bioactive molecules including drugs, proteins, and targeting ligands (32).

Another major challenge for radioactive nanoparticles is in optimization of their effectiveness to target specific disease phenotypes (39). Significant reports on radioactive nanomaterials used passive targeting only based on the enhanced permeation and retention effect, which is relying on the size, shape, surface charge, and circulation half-life of the nanoparticles. Although this can be therapeutically efficacious in some cases, this is by no means optimal for an imaging/diagnostic purpose. For example, the prolonged circulation half-life from a nanomaterial is a double-edged sword—although it can lead to a higher level of passive targeting to the tumor, it also causes prolonged exposure of the normal organs to the drug/radioisotope, which can give rise to undesired systemic toxicity. Active targeting is an approach that can enhance the preferential nanomaterial accumulation at disease site(s) via coupling with ligands that have selectivity and affinity toward diseased cells or tissues, or by a provided external stimulus (eg, a magnetic field) on a target cell/tissue spatial location (119). We can expect that significantly more research effort will be devoted to produce nanomaterials with active targeting capacity to improve multimodal image contrast. More specifically for oncological imaging, we believe that targeting of markers on tumor neovasculature will be more efficient for radioactive nanomaterials, as the size of many materials hinders their extravasation into the surrounding tumor parenchyma (120).

The majority of radioactive nanomaterials discussed in this paper have a hydrodynamic size range of 10–200 nm, which can cause persistent accumulation in the mononuclear phagocyte system (eg, liver and spleen). To ensure that a long-term safety profile can be achieved, careful radiation dosimetry and toxicological evaluation for each radioactive nanomaterial should be accomplished (121). In the meantime, suitable biological properties should be engineered into the design of the nanomaterial (eg, size/surface charge/degradability adjustment for fast renal clearance) in an effort to tune the in vivo distribution pattern to allow for injected contrast agents to be cleared within a reasonable period to meet subsequent FDA approval (122).

In summary, radioactive nanomaterials that can integrate multiple contrast agents into 1 single platform are important to realize real-time multimodality imaging. As multimodality imaging probes, radioactive nanomaterials should be able to provide for improved diagnostic accuracy. Continued research into the development of radioactive nanomaterials for imaging applications is anticipated to lead to, for example, radiolabeled IONPs that will be useful in simultaneous PET/MRI for early cancer diagnosis and disease staging. There are numerous opportunities and underexplored areas in radioactive nanomaterial research (eg, manganese nanomaterials), which we believe will serve as indispensable diagnostic and therapeutic tools in future medical applications. Overall, it is fully anticipated that continued advances in nanomaterials research will significantly improve clinical care and have a significant and positive impact on enhancing patient outcomes in the years ahead.

ACKNOWLEDGMENTS

This work is supported in part by the University of Michigan Department of Radiology, the Elsa U. Pardee Foundation, and the National Institutes of Health (NCI P01 CA085878).

Conflict of Interest: None reported.

REFERENCES

1. Weissleder R, Pittet MJ. Imaging in the era of molecular oncology. Nature. 2008;452(7187):580–589.
2. Kurtz DM, Gambhir SS. Tracking cellular and immune therapies in cancer. Adv Cancer Res. 2014;124:257–296.
3. Pysz MA, Gambhir SS, Willmann JK. Molecular imaging: current status and emerging strategies. Clin Radiol. 2010;65(7):500–516.
4. James ML, Gambhir SS. A molecular imaging primer: modalities, imaging agents, and applications. Physiol Rev. 2012;92(2):897–965.
5. Lee DE, Koo H, Sun IC, Ryu JH, Kim K, Kwon IC. Multifunctional nanoparticles for multimodal imaging and theragnosis. Chem Soc Rev. 2012;41(7):2656–2672.
6. Huang Y, He S, Cao W, Cai K, Liang XJ. Biomedical nanomaterials for imaging-guided cancer therapy. Nanoscale. 2012;4(20):6135–6149.
7. Jennings LE, Long NJ. 'Two is better than one'–probes for dual-modality molecular imaging. Chem Commun (Camb). 2009;(24):3511–3524.
8. Louie A. Multimodality imaging probes: design and challenges. Chem Rev. 2010;110(5):3146–3195.
9. Kim J, Piao Y, Hyeon T. Multifunctional nanostructured materials for multimodal imaging, and simultaneous imaging and therapy. Chem Soc Rev. 2009;38(2):372–390.
10. Culver J, Akers W, Achilefu. Multimodality molecular imaging with combined optical and SPECT/PET modalities. J Nucl Med. 2008;49(2):169–172.
11. de Rosales RT. Potential clinical applications of bimodal PET-MRI or SPECT-MRI agents. J Labelled Comp Radiopharm. 2014;57(4):298–303.
12. Deri MA, Zeglis BM, Francesconi LC, Lewis JS. PET imaging with ^{89}Zr: from radiochemistry to the clinic. Nucl Med Biol. 2013;40(1):3–14.
13. Anderson CJ, Ferdani R. Copper-64 radiopharmaceuticals for PET imaging of cancer: advances in preclinical and clinical research. Cancer Biother Radiopharm. 2009;24(4):379–393.
14. Ametamey SM, Honer M, Schubiger PA. Molecular imaging with PET. Chem Rev. 2008;108(5):1501–1516.
15. Townsend DW, Carney JP, Yap JT, Hall NC. PET/CT today and tomorrow. J Nucl Med. 2004;45(1):4S–14S.
16. Townsend DW. A combined PET/CT scanner: the choices. J Nucl Med. 2001;42(3):533–534.
17. Nishioka T, Shiga T, Shirato H, Tsukamoto E, Tsuchiya K, Kato T, Ohmori K, Yamazaki A, Aoyama H, Hashimoto S, Chang TC, Miyasaka K. Image fusion between ^{18}FDG-PET and MRI/CT for radiotherapy planning of oropharyngeal and nasopharyngeal carcinomas. Int J Rad Oncol Biol Phys. 2002;53(4):1051–1057.
18. Bar-Shalom R, Yefremov N, Guralnik L, Gaitini D, Frenkel A, Kuten A, Altman H, Keidar Z, Israel O. Clinical performance of PET/CT in evaluation of cancer: additional value for diagnostic imaging and patient management. J Nucl Med. 2003;44(8):1200–1209.
19. Pichler BJ, Judenhofer MS, Catana C, Walton JH, Kneilling M, Nutt RE, Siegel SB, Claussen CD, Cherry SR. Performance test of an LSO-APD detector in a 7-T MRI scanner for simultaneous PET/MRI. J Nucl Med. 2006;47(4):639–647.

20. Bouziotis P, Psimadas D, Tsotakos T, Stamopoulos D, Tsoukalas C. Radiolabeled iron oxide nanoparticles as dual-modality SPECT/MRI and PET/MRI agents. Curr Topics Med Chem. 2012;12(23):2694–2702.
21. Judenhofer MS, Wehrl HF, Newport DF, Catana C, Siegel SB, Becker M, Thielscher A, Kneilling M, Lichy MP, Eichner M, Klingel K, Reischl G, Widmaier S, Röcken M, Nutt RE, Machulla HJ, Uludag K, Cherry SR, Claussen CD, Pichler BJ. Simultaneous PET-MRI: a new approach for functional and morphological imaging. Nat Med. 2008;14(4):459–465.
22. Hofmann M, Pichler B, Schölkopf B, Beyer T. Towards quantitative PET/MRI: a review of MR-based attenuation correction techniques. Eur J Nucl Med Mol Imaging. 2009;36(1):93–104.
23. Antoch G, Bockisch A. Combined PET/MRI: a new dimension in whole-body oncology imaging? Eur J Nucl Med Mol Imaging. 2009;36(1):S113–S120.
24. Hussain T, Nguyen QT. Molecular imaging for cancer diagnosis and surgery. Adv Drug Deliv Rev. 2014;66:90–100.
25. Luo J, Wilson JD, Zhang J, Hirsch JI, Dorn HC, Fatouros PP, Shultz MD. A dual PET/MR imaging nanoprobe: ^{124}I labeled Gd_3N@ C_{80}. Appl Sci. 2012;2(2): 465–478.
26. Cowger T, Xie J. Polyaspartic acid coated iron oxide nanoprobes for PET/MRI imaging. Methods Mol Biol. 2013;1025:225–235.
27. Hahn MA, Singh AK, Sharma P, Brown SC, Moudgil BM. Nanoparticles as contrast agents for in-vivo bioimaging: current status and future perspectives. Anal Bioanal Chem. 2011;399(1):3–27.
28. Liang R, Wei M, Evans DG, Duan X. Inorganic nanomaterials for bioimaging, targeted drug delivery and therapeutics. Chem Commun (Camb). 2014;50(91): 14071–14081.
29. Barreto JA, O'Malley W, Kubeil M, Graham B, Stephan H, Spiccia L. Nanomaterials: applications in cancer imaging and therapy. Adv Mater. 2011;23(12): H18–H40.
30. Ai F, Ferreira CA, Chen F, Cai W. Engineering of radiolabeled iron oxide nanoparticles for dual-modality imaging. Wiley Interdiscip Rev Nanomed Nanobiotechnol. 2015. doi: 10.1002/wnan.1386. [Epub ahead of print].
31. Lee JH, Kim JW, Cheon J. Magnetic nanoparticles for multi-imaging and drug delivery. Mol Cell. 2013;35(4):274–284.
32. Liu Z, Kiessling K, Gätjens J. Advanced nanomaterials in multimodal imaging: design, functionalization, and biomedical applications. J Nanomater. 2009; 2010(2010):15.
33. Biju V. Chemical modifications and bioconjugate reactions of nanomaterials for sensing, imaging, drug delivery and therapy. Chem Soc Rev. 2014; 43(3):744–764.
34. Portney NG, Ozkan M. Nano-oncology: drug delivery, imaging, and sensing. Anal Bioanal Chem. 2006;384(3):620–630.
35. Ahmed N, Fessi H, Elaissari A. Theranostic applications of nanoparticles in cancer. Drug Discov Today. 2012;17(17-18):928–934.
36. Chen Y, Chen H, Shi J. In vivo bio-safety evaluations and diagnostic/therapeutic applications of chemically designed mesoporous silica nanoparticles. Adv Mater. 2013;25(23):3144–3176.
37. Alex S, Tiwari A. Functionalized gold nanoparticles: synthesis, properties and applications–a review. J Nanosci Nanotechnol. 2015;15(3):1869–1894.
38. Chen D, Dougherty CA, Zhu K, Hong H. Theranostic applications of carbon nanomaterials in cancer: focus on imaging and cargo delivery. J Control Release. 2015;210:230–245.
39. Hong H, Zhang Y, Sun J, Cai W. Molecular imaging and therapy of cancer with radiolabeled nanoparticles. Nano Today. 2009;4(5):399–413.
40. Gibson N, Holzwarth U, Abbas K, Simonelli F, Kozempel J, Cydzik I, Cotogno G, Bulgheroni A, Gilliland D, Ponti J, Franchini F, Marmorato P, Stamm H, Kreyling W, Wenk A, Semmler-Behnke M, Buono S, Maciocco L, Burgio N. Radiolabelling of engineered nanoparticles for in vitro and in vivo tracing applications using cyclotron accelerators. Arch Toxicol. 2011;85(7):751–773.
41. Black KC, Wang Y, Luehmann HP, Cai X, Xing W, Pang B, Zhao Y, Cutler CS, Wang LV, Liu Y, Xia. Radioactive ^{198}Au-doped nanostructures with different shapes for in vivo analyses of their biodistribution, tumor uptake, and intratumoral distribution. ACS Nano. 2014;8(5):4385–4394.
42. Wang Y, Liu Y, Luehmann H, Xia X, Wan D, Cutler C, Xia Y. Radioluminescent gold nanocages with controlled radioactivity for real-time in vivo imaging. Nano Lett. 2013;13(13):581–585.
43. Zhou M, Zhang R, Huang M, Lu W, Song S, Melancon MP, Tian M, Liang D, Li C. A chelator-free multifunctional [^{64}Cu] CuS nanoparticle platform for simultaneous micro-PET/CT imaging and photothermal ablation therapy. J Am Chem Soc. 2010;132(43):15351–15358.
44. Hu H, Huang P, Weiss OJ, Yan X, Yue X, Zhang MG, Tang Y, Nie L, Ma Y, Niu G, Wu K, Chen X. PET and NIR optical imaging using self-illuminating 64 Cu-doped chelator-free gold nanoclusters. Biomaterials. 2014;35(37):9868–9876.
45. Sun X, Cai W, Chen X. Positron emission tomography imaging using radiolabeled inorganic nanomaterials. Acc Chem Res. 2015;48(2):286–294.
46. Pichler BJ, Kolb A, Nägele T, Schlemmer HP. PET/MRI: paving the way for the next generation of clinical multimodality imaging applications. J Nucl Med. 2010;51(3):333–336.
47. Martinez-Möller A, Souvatzoglou M, Delso G, Bundschuh RA, Chefd'hotel C, Ziegler SI, Navab N, Schwaiger M, Nekolla SG. Tissue classification as a potential approach for attenuation correction in whole-body PET/MRI: evaluation with PET/CT data. J Nucl Med. 2009;50(4):520–526.
48. Keereman V, Fierens Y, Broux T, De Deene Y, Lonneux M, Vandenberghe S. MRI-based attenuation correction for PET/MRI using ultrashort echo time sequences. J Nucl Med. 2010;51(5):812–818.
49. Glaus C, Rossin R, Welch MJ, Bao G. In vivo evaluation of ^{64}Cu-labeled magnetic nanoparticles as a dual-modality PET/MR imaging agent. Bioconjug Chem. 2010;21(4):715–722.
50. Pablico-Lansigan MH, Situ SF, Samia AC. Magnetic particle imaging: advancements and perspectives for real-time in vivo monitoring and image-guided therapy. Nanoscale. 2013;5(10):4040–4055.
51. Bouziotis P, Psimadas D, Tsotakos T, Stamopoulos D, Tsoukalas C. Radiolabeled iron oxide nanoparticles as dual-modality SPECT/MRI and PET/MRI agents. Curr Top Med Chem. 2012;12(23):2694–2702.
52. Zhang Y, Hong H, Cai W. PET tracers based on Zirconium-89. Curr Radiopharm. 2011;4(2):131–139.
53. Thorek DL, Ulmert D, Diop NF, Lupu ME, Doran MG, Huang R, Abou DS, Larson SM, Grimm J. Non-invasive mapping of deep-tissue lymph nodes in live animals using a multimodal PET/MRI nanoparticle. Nat Commun. 2014;5:3097.
54. Choi JS, Park JC, Nah H, Woo S, Oh J, Kim KM, Cheon GJ, Chang Y, Yoo J, Cheon J. A hybrid nanoparticle probe for dual-modality positron emission tomography and magnetic resonance imaging. Angew Chem Int Ed Engl. 2008; 47(33):6259–6262.
55. Torres Martin de Rosales R, Tavaré R, Paul RL, Jauregui-Osoro M, Protti A, Glaria A, Varma G, Szanda I, Blower PJ. Synthesis of ^{64}Cu(II)-bis(dithiocarbamatebisphosphonate) and its conjugation with superparamagnetic iron oxide nanoparticles: in vivo evaluation as dual-modality PET-MRI agent. Angew Chem Int Ed Engl. 2011;50(4):5509–5513.
56. Chakravarty R, Valdovinos HF, Chen F, Lewis CM, Ellison PA, Luo H, Meyerand ME, Nickles RJ, Cai W. Intrinsically germanium-69-labeled iron oxide nanoparticles: synthesis and in-vivo dual-modality PET/MR imaging. Adv Mater. 2014; 26(30):5119–5123.
57. Chen F, Ellison PA, Lewis CM, Hong H, Zhang Y, Shi S, Hernandez R, Meyerand ME, Barnhart TE, Cai W. Chelator-free synthesis of a dual-modality PET/MRI agent. Angew Chem Int Ed Engl. 2013;52(50):13319–13323.
58. Xie J, Chen K, Huang J, Lee S, Wang J, Gao J, Li X, Chen X. PET/NIRF/MRI triple functional iron oxide nanoparticles. Biomaterials. 2010;31(11):3016–3022.
59. Yang X, Hong H, Grailer JJ, Rowland IJ, Javadi A, Hurley SA, Xiao Y, Yang Y, Zhang Y, Nickles RJ, Cai W, Steeber DA, Gong S. cRGD-functionalized, DOX-conjugated, and ^{64}Cu-labeled superparamagnetic iron oxide nanoparticles for targeted anticancer drug delivery and PET/MR imaging. Biomaterials. 2011; 32(17):4151–4160.
60. Lee HY, Li Z, Chen K, Hsu AR, Xu C, Xie J, Sun S, Chen X. PET/MRI dual-modality tumor imaging using arginine-glycine-aspartic (RGD)-conjugated radiolabeled iron oxide nanoparticles. J Nucl Med. 2008;49(8):1371–1379.
61. Cui X, Belo S, Krüger D, Yan Y, de Rosales RT, Jauregui-Osoro M, Ye H, Su S, Mathe D, Kovács N, Horváth I, Semjeni M, Sunassee K, Szigeti K, Green MA, Blower PJ. Aluminium hydroxide stabilised $MnFe_2O_4$ and Fe_3O_4 nanoparticles as dual-modality contrasts agent for MRI and PET imaging. Biomaterials. 2014; 35(22):5840–5846.
62. Liu T, Shi S, Liang C, Shen S, Cheng L, Wang C, Song X, Goel S, Barnhart TE, Cai W, Liu Z. Iron oxide decorated MoS_2 nanosheets with double PEGylation for chelator-free radiolabeling and multimodal imaging guided photothermal therapy. ACS Nano. 2015;9(1):950–960.
63. Borra RJ, Cho HS, Bowen SL, Attenberger U, Arabasz G, Catana C, Josephson L, Rosen BR, Guimaraes AR, Hooker JM. Effects of ferumoxytol on quantitative PET measurements in simultaneous PET/MR whole-body imaging: a pilot study in a baboon model. EJNMMI Phys. 2015;2(1):6.
64. Kim TJ, Chae KS, Chang Y, Lee GH. Gadolinium oxide nanoparticles as potential multimodal imaging and therapeutic agents. Curr Top Med Chem. 2013; 13(4):422–433.
65. Bouzigues C, Gacoin T, Alexandrou A. Biological applications of rare-earth based nanoparticles. ACS Nano. 2011;5(11):8488–8505.
66. Hu H, Li D, Liu S, Wang M, Moats R, Conti PS, Li Z. Integrin alpha2beta1 targeted $GdVO_4$:Eu ultrathin nanosheet for multimodal PET/MR imaging. Biomaterials. 2014;35(30):8649–8658.
67. Cheng K, Yang M, Zhang R, Qin C, Su X, Cheng Z. Hybrid nanotrimers for dual T1 and T2-weighted magnetic resonance imaging. ACS Nano. 2014; 8(10):9884–9896.

68. Abou DS, Thorek DL, Ramos NN, Pinkse MW, Wolterbeek HT, Carlin SD, Beattie BJ, Lewis JS. ^{89}Zr-labeled paramagnetic octreotide-liposomes for PET-MR imaging of cancer. Pharm Res. 2013;30(3):878–888.
69. Kaittanis C, Shaffer TM, Bolaender A, Appelbaum Z, Appelbaum J, Chiosis G, Grimm J. Multifunctional MRI/PET nanobeacons derived from the in situ self-assembly of translational polymers and clinical cargo through coalescent intermolecular forces. Nano Lett. 2015;15(12):8032–8043.
70. Jacobs KE, Behera D, Rosenberg J, Gold G, Moseley M, Yeomans D, Biswal S. Oral manganese as an MRI contrast agent for the detection of nociceptive activity. NMR Biomed. 2012;25(4):563–569.
71. Crossgrove J, Zheng W. Manganese toxicity upon overexposure. NMR Biomed. 2004;17(8):544–553.
72. Huang J, Xie J, Chen K, Bu L, Lee S, Cheng Z, Li X, Chen X. HSA coated MnO nanoparticles with prominent MRI contrast for tumor imaging. Chem Commun (Camb). 2010;46(36):6684–6686.
73. Graves SA, Hernandez R, Fonslet J, England CG, Valdovinos HF, Ellison PA, Barnhart TE, Elema DR, Theuer CP, Cai W, Nickles RJ, Severin GW. Novel preparation methods of ^{52}Mn for immunoPET imaging. Bioconjug Chem. 2015; 26(10):2118–2124.
74. Hao Y, Wang L, Zhang B, Zhao H, Niu M, Hu Y, Zheng C, Zhang H, Chang J, Zhang Z, Zhang Y. Multifunctional nanosheets based on folic acid modified manganese oxide for tumor-targeting theranostic application. Nanotechnology. 2016;27(2):025101.
75. Chen F, Hong H, Shi S, Goel S, Valdovinos HF, Hernandez R, Theuer CP, Barnhart TE, Cai W. Engineering of hollow mesoporous silica nanoparticles for remarkably enhanced tumor active targeting efficacy. Sci Rep. 2014;4:5080.
76. Guo J, Hong H, Chen G, Shi S, Zheng Q, Zhang Y, Theuer CP, Barnhart TE, Cai W, Gong S. Image-guided and tumor-targeted drug delivery with radiolabeled unimolecular micelles. Biomaterials. 2013;34(33):8323–8332.
77. Xiao Y, Hong H, Javadi A, Engle JW, Xu W, Yang Y, Zhang Y, Barnhart TE, Cai W, Gong S. Multifunctional unimolecular micelles for cancer-targeted drug delivery and positron emission tomography imaging. Biomaterials. 2012; 33(11):3071–3082.
78. Thorek DL, Robertson R, Bacchus WA, Hahn J, Rothberg J, Beattie BJ, Grimm J. Cerenkov imaging - a new modality for molecular imaging. Am J Nucl Med Mol Imaging. 2012;2(2):163–173.
79. Chen K, Li ZB, Wang H, Cai W, Chen X. Dual-modality optical and positron emission tomography imaging of vascular endothelial growth factor receptor on tumor vasculature using quantum dots. Eur J Nucl Med Mol imaging. 2008; 35(12):2235–2244.
80. Cai W, Chen K, Li ZB, Gambhir SS, Chen X. Dual-function probe for PET and near-infrared fluorescence imaging of tumor vasculature. J Nucl Med. 2007; 48(11):1862–1870.
81. Ducongé F, Pons T, Pestourie C, Hérin L, Thézé B, Gombert K, Mahler B, Hinnen F, Kühnast B, Dollé F, Dubertret B, Tavitian B. Fluorine-18-labeled phospholipid quantum dot micelles for in vivo multimodal imaging from whole body to cellular scales. Bioconjug Chem. 2008;19(9):1921–1926.
82. Park YI, Lee KT, Suh YD, Hyeon T. Upconverting nanoparticles: a versatile platform for wide-field two-photon microscopy and multi-modal in vivo imaging. Chem Soc Rev. 2015;44(6):1302–1317.
83. Liu Q, Chen M, Sun Y, Chen G, Yang T, Gao Y, Zhang X, Li F. Multifunctional rare-earth self-assembled nanosystem for tri-modal upconversion luminescence/ fluorescence/positron emission tomography imaging. Biomaterials. 2011; 32(32):8243–8253.
84. Hong H, Wang F, Zhang Y, Graves SA, Eddine SB, Yang Y, Theuer CP, Nickles RJ, Wang X, Cai W. Red fluorescent zinc oxide nanoparticle: a novel platform for cancer targeting. ACS Appl Mater Interfaces. 2015;7(5):3373–3381.
85. Nahrendorf M, Keliher E, Marinelli B, Waterman P, Feruglio PF, Fexon L, Pivovarov M, Swirski FK, Pittet MJ, Vinegoni C, Weissleder R. Hybrid PET-optical imaging using targeted probes. Proc Nat Acad Sci U S A. 2010;107(17): 79105.
86. Chen F, Nayak TR, Goel S, Valdovinos HF, Hong H, Theuer CP, Barnhart TE, Cai W. In vivo tumor vasculature targeted PET/NIRF imaging with TRC105(Fab)-conjugated, dual-labeled mesoporous silica nanoparticles. Mol Pharm. 2014; 11(11):4007–4014.
87. Bradbury MS, Phillips E, Montero PH, Cheal SM, Stambuk H, Durack JC, Sofocleous CT, Meester RJ, Wiesner U, Patel S. Clinically-translated silica nanoparticles as dual-modality cancer-targeted probes for image-guided surgery and interventions. Integr Biol (Camb). 2013;5(1):74–86.
88. Phillips E, Penate-Medina O, Zanzonico PB, Carvajal RD, Mohan P, Ye Y, Humm J, Gönen M, Kalaigian H, Schöder H, Strauss HW, Larson SM, Wiesner U, Bradbury MS. Clinical translation of an ultrasmall inorganic optical-PET imaging nanoparticle probe. Sci Transl Med. 2014;6(260):260ra149.
89. Sun X, Huang X, Guo J, Zhu W, Ding Y, Niu G, Wang A, Kiesewetter DO, Wang ZL, Sun S, Chen X. Self-illuminating ^{64}Cu-doped CdSe/ZnS nanocrystals for in vivo tumor imaging. J Am Chem Soc. 2014;136(5):1706–1709.
90. Guo W, Sun X, Jacobson O, Yan X, Min K, Srivatsan A, Niu G, Kiesewetter DO, Chang J, Chen X. Intrinsically radioactive [^{64}Cu]CuInS/ZnS quantum dots for PET and optical imaging: improved radiochemical stability and controllable Cerenkov luminescence. ACS Nano. 2015;9(1):488–495.
91. Thorek DL, Riedl CC, Grimm J. Clinical Cerenkov luminescence imaging of ^{18}F-FDG. J Nucl Med. 2014;55(1):95–98.
92. Zhang Y, Hong H, Cai W. Imaging with Raman spectroscopy. Curr Pharm Biotechnol. 2010;11(6):654–661.
93. Zavaleta CL, Hartman KB, Miao Z, James ML, Kempen P, Thakor AS, Nielsen CH, Sinclair R, Cheng Z, Gambhir SS. Preclinical evaluation of Raman nanoparticle biodistribution for their potential use in clinical endoscopy imaging. Small. 2011;7(15):2232–2240.
94. Zhang Y, Hong H, Cai W. Photoacoustic imaging. Cold Spring Harb Protoc. 2011;2011(9):pii: pdb.top065508.
95. Cheng K, Kothapalli SR, Liu H, Koh AL, Jokerst JV, Jiang H, Yang M, Li J, Levi J, Wu JC, Gambhir SS, Cheng Z. Construction and validation of nano gold tripods for molecular imaging of living subjects. J Am Chem Soc. 2014;136(9): 3560–3571.
96. Yang M, Fan Q, Zhang R, Cheng K, Yan J, Pan D, Ma X, Lu A, Cheng Z. Dragon fruit-like biocage as an iron trapping nanoplatform for high efficiency targeted cancer multimodality imaging. Biomaterials. 2015;69:30–37.
97. Park JC, Yu MK, An GI, Park SI, Oh J, Kim HJ, Kim JH, Wang EK, Hong IH, Ha YS, Choi TH, Jeong KS, Chang Y, Welch MJ, Jon S, Yoo J. Facile preparation of a hybrid nanoprobe for triple-modality optical/PET/MR imaging. Small. 2010;6(24):2863–2868.
98. Kang KW. Preliminary pre-clinical results and overview on PET/MRI/fluorescent molecular imaging. Open Nucl Med J. 2010;2:153–156.
99. Yang M, Cheng K, Qi S, Liu H, Jiang Y, Jiang H, Li J, Chen K, Zhang H, Cheng Z. Affibody modified and radiolabeled gold–iron oxide hetero-nanostructures for tumor PET, optical and MR imaging. Biomaterials. 2013;34(11):2796–2806.
100. Xie J, Chen K, Huang J, Lee S, Wang J, Gao J, Li X, Chen X. PET/NIRF/MRI triple functional iron oxide nanoparticles. Biomaterials. 2010;31(11):3016–3022.
101. Huang X, Zhang F, Lee S, Swierczewska M, Kiesewetter DO, Lang L, Zhang G, Zhu L, Gao H, Choi HS, Niu G, Chen X. Long-term multimodal imaging of tumor draining sentinel lymph nodes using mesoporous silica-based nanoprobes. Biomaterials. 2012;33(17):4370–4378.
102. Cui X, Mathe D, Kovács N, Horváth I, Jauregui-Osoro M, Torres Martin de Rosales R, Mullen GE, Wong W, Yan Y, Krüger D, Khlobystov AN, Gimenez-Lopez M, Semjeni M, Szigeti K, Veres DS, Lu H, Hernández I, Gillin WP, Protti A, Petik KK, Green MA, Blower PJ. Synthesis, characterization, and application of core–shell $Co_{0.16}Fe_{2.84}O_4$@ $NaYF_4$ (Yb, Er) and Fe_3O_4@ $NaYF_4$ (Yb, Tm) nanoparticle as trimodal (MRI, PET/SPECT, and Optical) imaging agents. Bioconjug Chem. 2016;27(2):319–328 (Epub 2015 Aug 14).
103. Rieffel J, Chen F, Kim J, Chen G, Shao W, Shao S, Chitgupi U, Hernandez R, Graves SA, Nickles RJ, Prasad PN, Kim C, Cai W, Lovell JF. Hexamodal imaging with porphyrin-phospholipid-coated upconversion nanoparticles. Adv Mater. 2015;27(10):1785–1790.
104. Eckelman WC. Unparalleled contribution of technetium-99m to medicine over 5 decades. JACC Cardiovasc Imaging. 2009;2(3):364–368.
105. Berman DS, Kiat H, Van Train K, Friedman JD, Wang FP, Germano G. Dual-isotope myocardial perfusion SPECT with rest thallium-201 and stress Tc-99m sestamibi. Cardiol Clin. 1994;12(2):261–270.
106. Madru R, Kjellman P, Olsson F, Wingårdh K, Ingvar C, Ståhlberg F, Olsrud J, Lätt J, Fredriksson S, Knutsson L, Strand SE. ^{99m}Tc-labeled superparamagnetic iron oxide nanoparticles for multimodality SPECT/MRI of sentinel lymph nodes. J Nucl Med. 2012;53(3):459–463.
107. Lijowski M, Caruthers S, Hu G, Zhang H, Scott MJ, Williams T, Erpelding T, Schmieder AH, Kiefer G, Gulyas G, Athey PS, Gaffney PJ, Wickline SA, Lanza GM. High sensitivity: high resolution SPECT-CT/MR molecular imaging of angiogenesis in the Vx2 model. Invest Radiol. 2009;44(1):15–22.
108. Zielhuis SW, Seppenwoolde JH, Mateus VA, Bakker CJ, Krijger GC, Storm G, Zonnenberg BA, van het Schip AD, Koning GA, Nijsen JF. Lanthanide-loaded liposomes for multimodality imaging and therapy. Cancer Biother Radiopharm. 2006;21(5):520–527.
109. Lee HY, Li Z, Chen K, Hsu AR, Xu C, Xie J, Sun S, Chen X. PET/MRI dual-modality tumor imaging using arginine-glycine-aspartic (RGD)–conjugated radiolabeled iron oxide nanoparticles. J Nucl Med. 2008;49(8):1371–1379.
110. Torres Martin de Rosales R, Tavaré R, Glaria A, Varma G, Protti A, Blower PJ. ^{99m}Tc-bisphosphonate-iron oxide nanoparticle conjugates for dual-modality biomedical imaging. Bioconjugate Chem. 2011;22(3):455–465.
111. Sandiford L, Phinikaridou A, Protti A, Meszaros LK, Cui X, Yan Y, Frodsham G, Williamson PA, Gaddum N, Botnar RM, Blower PJ, Green MA, de Rosales RT. Bisphosphonate-anchored PEGylation and radiolabeling of superparamagnetic iron oxide: long-circulating nanoparticles for in vivo multimodal (T_1 MRI-SPECT) imaging. ACS Nano. 2012;7(1):500–512.

112. Wang JT-W, Cabana L, Bourgognon M, Kafa H, Protti A, Venner K, Shah AM, Sosabowski J, Mather SJ, Roig A, Ke X, Tendeloo GV, de Rosales RT, Tobias G, Al-Jamal KT. Magnetically decorated multiwalled carbon nanotubes as dual MRI and SPECT contrast agents. Adv Funct Mater. 2014;24(13):1880–1894.
113. Kryza D, Taleb J, Janier M, Marmuse L, Miladi I, Bonazza P, Louis C, Perriat P, Roux S, Tillement O, Billotey C. Biodistribution study of nanometric hybrid gadolinium oxide particles as a multimodal SPECT/MR/optical imaging and theragnostic agent. Bioconjug Chem. 2011;22(6):1145–1152.
114. Zhang R, Xiong C, Huang M, Zhou M, Huang Q, Wen X, Liang D, Li C. Peptide-conjugated polymeric micellar nanoparticles for dual SPECT and optical imaging of EphB4 receptors in prostate cancer xenografts. Biomaterials. 2011; 32(25):5872–5879.
115. Mitchell N, Kalber TL, Cooper MS, Sunassee K, Chalker SL, Shaw KP, Ordidge KL, Badar A, Janes SM, Blower PJ, Lythgoe MF, Hailes HC, Tabor AB. Incorporation of paramagnetic, fluorescent and PET/SPECT contrast agents into liposomes for multimodal imaging. Biomaterials. 2013;34(4):1179–1192.
116. Guo Y, Yuan H, Claudio NM, Kura S, Shakerdge N, Mempel TR, Bacskai BJ, Josephson L. PEG-like nanoprobes: multimodal, pharmacokinetically and optically tunable nanomaterials. Plos One. 2014;9(4):e95406.
117. Ellison PA, Barnhart TE, Chen F, Hong H, Zhang Y, Theuer CP1, Cai W, Nickles RJ, DeJesus OT. High yield production and radiochemical isolation of isotopically pure arsenic-72 and novel radioarsenic labeling strategies for the development of theranostic radiopharmaceuticals. Bioconjug Chem. 2016;27(1): 179–188.
118. Al Faraj A, Alotaibi B, Shaik AP, Shamma KZ, Al Jammaz I, Gerl J. Sodium-22-radiolabeled silica nanoparticles as new radiotracer for biomedical applications: in vivo positron emission tomography imaging, biodistribution, and biocompatibility. Int J Nanomedicine. 2015;10:6293–6302.
119. Yang Y, Yu C. Advances in silica based nanoparticles for targeted cancer therapy. Nanomedicine. 2015 pii: S1549-9634(15)00585-7 [Epub ahead of print].
120. Hong H, Chen F, Zhang Y, Cai W. New radiotracers for imaging of vascular targets in angiogenesis-related diseases. Adv Drug Deliv Rev. 2014;76:2–20.
121. Khalili Fard J, Jafari S, Eghbal MA. A review of molecular mechanisms involved in toxicity of nanoparticles. Adv Pharm Bull. 2015;5(4):447–454.
122. Choi HS, Liu W, Liu F, Nasr K, Misra P, Bawendi MG, Frangioni JV. Design considerations for tumour-targeted nanoparticles. Nat Nanotechnol. 2010;5(1): 42–47.